Solar RRL
www.solar-rrl.com

Improving Performance of Bifacial-Grid III–V Solar Cells Bonded on Glass by Selective Contact Annealing

Caixia Li, He Wang, Ziheng Liu, Hongliang Guo, Pengfei Zhang, Germain Rey, Jialiang Huang, Peng Gao, Qiang Sun, Wudi Zhang, Nicholas Ekins-Daukes, and Xiaojing Hao*

Selective contact annealing is developed to improve the performance of bifacial-grid III–V top cells bonded on glass by epoxy resin for Si-based tandem solar cells. The annealing method can minimize the damage to the bonding layer and is compatible with the industrial evaporation technique for contact fabrication. The improvement of the front contact quality by selective annealing treatments is demonstrated through optical and electrical characterization which shows a significantly enhanced III–V device performance. Furthermore, a fitting model is established to reveal the mechanism underlying the performance improvement through the reduction of contact resistances and the bad contact area. Herein, an effective annealing approach to fabricate high-quality metal–semiconductor contacts for devices with poor thermal resistivity is demonstrated, which can be used in polymer-bonded top cells in Si-based tandem solar cells and other flexible optoelectronic devices on polymer substrates.

1. Introduction

In recent years, a noticeable amount of research effort has been devoted to Si-based multijunction solar cells (MJSCs), which is a promising solution to achieving high-performance and low-cost photovoltaic devices. As III–V cells have suitable properties acting as top cells, a series of strategies have been investigated to fabricate III–V/Si tandem cells including direct growth,[1–3] wafer bonding,[4,5] and mechanical stacking.[6,7] Although the growth techniques based on GaAs substrate have been intensively investigated,[8–10] due to the mismatched lattice constants and thermal expansion coefficients between III–V and Si, the efficiency of III–V/Si MJSCs by the direct growth approach is still limited to 24.3%.[11] The surface-activated wafer bonding method can overcome the lattice mismatch issue and has achieved an efficiency of 34.1%.[5] However, this approach has a critical requirement of smooth particle-free surfaces with root-mean-square roughness values below 1 nm.[12] In contrast, the mechanical stacking method relieves the restriction of lattice and current mismatch between III–V and Si, places no requirement on subcell surface roughness, and eliminates the tunnel diode between subcells. The highest efficiency III–V/Si MJSC of 35.9% has been achieved through mechanically stacking GaInP/GaAs//Si triple-junction solar cells.[7]

In mechanically stacked III–V/Si MJSCs, the fabrication of high-quality front contact for III–V top cell bonded on transparent substrate is challenging due to the use of adhesive and transparent polymer bonding layer between the III–V cell and the glass substrate. After bonding and substrate removing process, the GaInP surface is accessible for front contact deposition. The fabrication of high-quality front contact using the industrial evaporation method usually requires contact annealing to form alloy, allowing the reduction of the contact resistance (R_c) between the metal grid and the semiconductor.[13–15] However, such conventional annealing treatment at 350 °C for a long duration is not compatible with the polymer bonding layer with poor thermal resistivity. The high-temperature treatment will decompose the polymer inducing bubble formation and therefore damaging the III–V cell. Electroplating of Au contact has been suggested as an alternative to obtaining good metal contacts for III–V cells bonded on glass.[7] But the electroplating of the Au contact is a complicated process and the liquid waste generated during the electroplating process shows environmental risk.[16,17] Therefore, a proper annealing treatment compatible with the industrial evaporation without damaging the polymer bonding layer underneath is required to obtain high-quality front contact for the III–V top cells.

To address the issues mentioned earlier, in this work, selective contact annealing using rapid thermal processing (RTP) or laser annealing has been developed to fabricate high-quality front contact for bifacial-grid III–V top cells bonded on glass. RTP can produce a rapid while well-controlled heating process[18] and thus is widely used to carry out thermal recrystallization.[19,20] Laser annealing with good selectivity has been used for reducing material defects in thin-film cells[21–23] and localized annealing

C. Li, Z. Liu, P. Zhang, G. Rey, J. Huang, N. Ekins-Daukes, X. Hao
School of Photovoltaic and Renewable Energy Engineering
University of New South Wales (UNSW)
Sydney, NSW 2052, Australia
E-mail: Ziheng.liu@unsw.edu.au

H. Wang, H. Guo, P. Gao, Q. Sun, W. Zhang
Solar Cell Research Laboratory
Tianjin Institute of Power Sources
Tianjin 300381, China

The ORCID identification number(s) for the author(s) of this article can be found under https://doi.org/10.1002/solr.202100438.

DOI: 10.1002/solr.202100438

for flexible thin-film transistors.[24] This work takes advantage of these above features of RTP and laser annealing to develop selective annealing approaches, and thus achieving high-quality front contact all over the device and subsequently improved cell performance.

Multiple characterization methods including the circular transmission line model (CTLM), electroluminescence (EL) imaging, photoluminescence (PL) imaging, and IV measurements indicate a noticeable decrease in R_c by selective annealing, which further contributes to the improvement of the device performance. Furthermore, numerical modeling has been conducted to investigate the performance improvement mechanism, and the reduction in R_c over the device after the contact annealing is verified. Selective contact annealing developed in this work offers a solution for large-scale production of high-quality bifacial-grid III–V cells on glass for Si-based MJSCs and provides feasible routes for the fabrication of flexible semiconductor devices on polymer substrates.

2. Experimental Section

A typical fabrication scheme of III–V cell on glass is shown in **Figure 1**, which involves a wafer-level layer transfer, making it a potential method for large-scale production. The GaInP/GaAs dual cells were grown inverted by metalorganic vapor phase epitaxy (MOVPE) on 4 in. GaAs substrates. After growth, on the 400 nm GaAs back cap layer, multiple stacks of metal grids of Au/Ge/Ag/Au were evaporated as back contacts and annealed by the conventional sintering at 350 °C for 30 min. Subsequently, an antireflection coating (ARC) layer was deposited on the backside of the cell to improve the optical transmission. The cell was then bonded onto a glass substrate by a highly transparent commercial epoxy (epo-tek 301) to minimize the optical loss for Si bottom cell. After the substrate removal by wet-chemical etching, the cap layer at the front side of the cell structure was accessible for front metal grids evaporation. Selective front contact annealing by either RTP or laser was then applied, followed by ARC deposition to finish the device fabrication. The detailed cell process method is described in the Supporting Information.

For the RTP annealing, a commercial system (AS-One 100) with halogen tubular lamps was used. The III–V cell was placed on the stage with the front metal contact facing the lamps. Considering the low thermal tolerance of the polymer, the temperature profiles and heating durations of RTP treatment were optimized to anneal metal grids with minimum damage on the polymer bonding layer. A slow ramping rate of 0.5 °C s^{-1} was used to avoid the delamination problem arising from the mismatch between thermal expansion coefficients of polymer and III–V materials.[25] As the significant weight loss of the polymer material at temperatures above 200 °C will lead to peeling off of the III–V cell, the RTP treatment process with a low annealing temperature of 200 °C and a short duration of 10 s was chosen. To compensate for the low temperature and short duration, multiple cycles of RTP treatments were conducted with the temperature profile shown in Figure S2, Supporting Information. The laser annealing was conducted using a Lissotschenko Mikrooptick GmbH (LIMO) continuous-wave diode laser with line-focus optics. A linear laser beam (12 mm × 270 μm) at 808 nm was applied on the front surface of III–V cells which were placed on a preheated stage with a surface temperature of 100 °C. The laser scan speed was 800 mm min^{-1}, leading to an exposure time of 20 ms. An optimized laser dose of 12 J cm^{-2} was set to effectively anneal the front contact meanwhile protecting the polymer bonding layer.

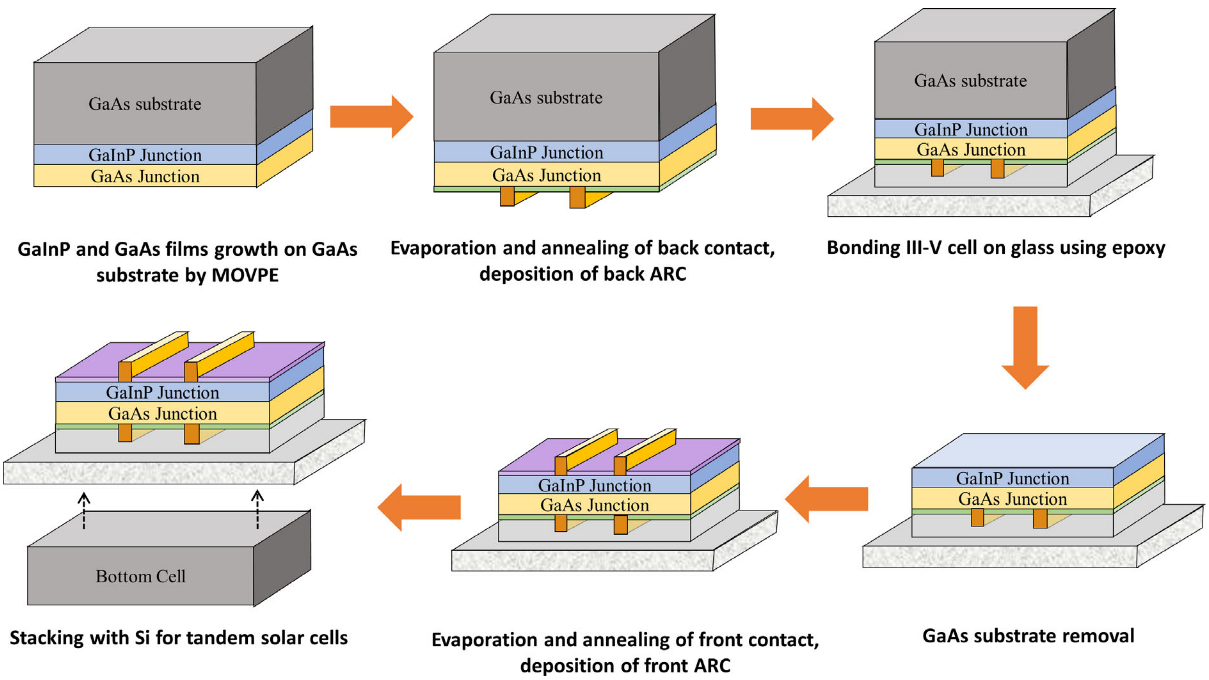

Figure 1. Fabrication flow of GaInP/GaAs cell with bifacial grid fingers bonded on glass for III–V/Si MJSCs.

Multiple characterizations were carried out to evaluate the performance of contact and cell after annealing treatments. For spatially resolved loss analysis of metal grids performance, EL and PL imaging were used. The luminescence signal was detected with a 4-megapixel silicon complementary metal-oxide–semiconductor camera. The PL excitation was provided by a commercial 300 W 640 nm light-emitting diode (LED) fitted with a short-pass filter, whose intensity was monitored by a calibrated silicon sensor. A set of bandpass optical filters were placed between the sample and the camera to prevent the capturing of LED light reflected from the sample. For the EL imaging, the III–V cell was forward biased by a DC power supply. Filters of band block 660–880 nm assembled with short pass 750 nm were used to capture the luminescence from GaInP and a filter of bandpass 730–980 nm was applied for GaAs junction. The CTLM was conducted to measure the specific contact resistance of the metal grids.[26] The designed contact pattern with varying exposed semiconductor spacing from 40 to 200 μm on the n-type GaAs cap layer (carrier concentration of $3 \times 10^{19}\,\text{cm}^{-3}$) was utilized. The electrical performance of cells before and after annealing was evaluated by IV measurement using a solar simulator (PV Measurement Inc. Oriel model 94023A). The numerical simulation model was established based on equivalent electrical circuits, and equations were solved by the numerical method in MATLAB.

3. Results and Discussion

3.1. Device Characterization and Optimization

The bifacial-grid III–V cells bonded on glass without front contact annealing showed poor IV performance, especially a low fill factor (FF) of 60%. EL and PL imaging measurements were used to investigate the cause for low FF. As shown in **Figure 2**a,b, the EL patterns of GaInP and GaAs junctions were obtained, respectively, under a forward bias voltage of 2.5 V. In addition to several dark line-shaped regions (indicated by white circles) corresponding to the recombination from mechanical scratches induced during the cell transferring process, the absence of EL emission at the edge region is observed for the GaInP top junction. Possible reasons for the inactive area in the EL image include shunt,[27] nonradiative recombination, and poor contact quality[28] in the device.

The shunt issue can be excluded as the EL image of the GaAs junction in Figure 2b does not show an obvious leakage current of shunts at the same location of inactive GaInP. The slight shunt-point marked in the black circle will not make an obvious impact on the device performance during the light IV characterization.[27] Furthermore, the nonradiative recombination will lead to lower Fermi-level separation and hence lower intensity of emission and it can be ruled out in this situation as the dark region of EL image with the low local voltage was not observed in the PL imaging, as shown in Figure 2c. In addition, the rear contact treated by traditional furnace annealing demonstrates good performance as the EL signal is captured at the edge region of the GaAs junction, which can be explained by the lateral conduction from multiple deep doped layers within the tunnel junction. Therefore, based on the analysis of EL and PL results, the poor performance of the device can be mainly attributed to the untreated front contact.

The untreated front contacts might cause high contact resistance (R_c).[13,14] The high R_c of contact may be related to the bad contact between metal grids and the semiconductor cap layer, where a layer of space charge near the semiconductor surface blocks the transportation of electrons.[29] This might be the reason for the dark region in the EL image of GaInP. The impacts of selective annealing on R_c and the cell performance are characterized and simulated to evaluate the effectiveness of annealing treatments in the following sections.

The accelerated metal diffusion by thermal annealing can effectively address the issue of low-quality front contact of the device.[13] To minimize the impact of annealing on the polymer bonding layer, RTP annealing with the advantages of short annealing duration and selectively heating from the top side of the device is used for front contact treatment. The impact of the RTP annealing on the device is demonstrated by the EL imaging of the GaInP junction. As shown in **Figure 3**a–c, after 10 cycles of RTP annealing at 200 °C for 10 s each cycle, the dark area near the busbar possibly due to the high R_c is eliminated, and the active area of the cell is significantly expanded. After another 20 cycles of RTP annealing, a slight expansion of the active area toward the end of metal grids is observed. The EL images demonstrate that the cyclic RTP annealing significantly improves the overall performance of the front contact.

To investigate the influence of RTP annealing on contact resistance, the CTLM is carried out to measure the specific contact

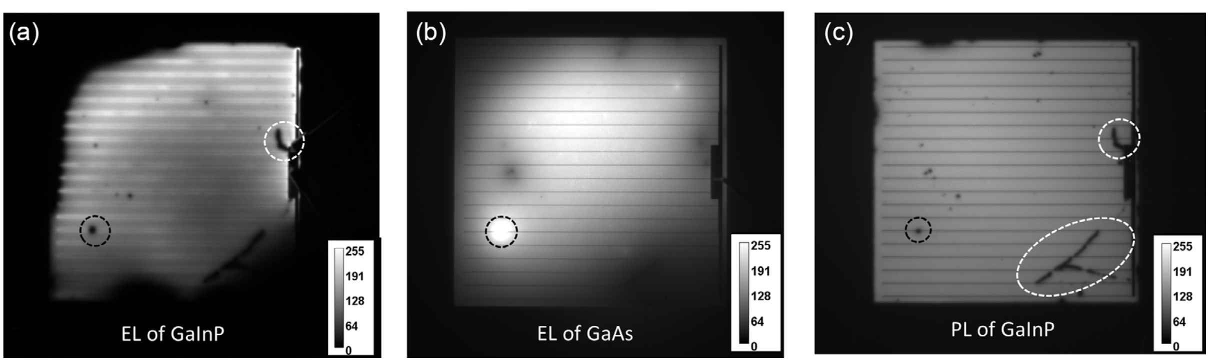

Figure 2. EL images of a) GaInP junction, b) GaAs junction, and c) PL image of the GaInP junction. The size of the cell is $2 \times 2\,\text{cm}^2$. White circles indicate mechanical scratches and black circles indicate shunts.

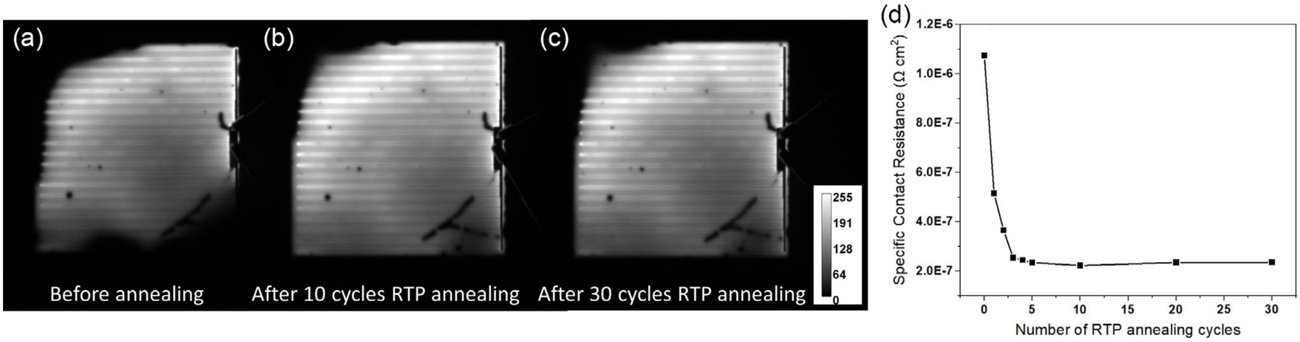

Figure 3. a–c) EL images of GaInP junction before and after cyclic RTP annealing. d) The specific contact resistance of Au/Ge/Ag/Au contact on n-type GaAs versus the number of RTP annealing cycles.

resistance. As shown in Figure 3d, after 10 cycles of RTP annealing, the specific contact resistance decreases from 1.09×10^{-6} to $2.00 \times 10^{-7}\ \Omega\text{cm}^2$ which is low enough for III–V photovoltaic devices.[30] The additional 20 cycles of RTP annealing cycles did not bring too much change in the specific contact resistance. The CTLM result indicates that the high contact resistance issue can be effectively addressed by RTP annealing. This agrees with the elimination of the dark area near the bus bar in the EL image after 10 cycles of RTP annealing in Figure 3b. It is worth noting that the contact area during the CTLM measurement is far smaller than the device area and the EL image indicates the nonuniform distribution of the contact resistance over the device. This suggests that the 10 cycles of RTP annealing might be not enough to realize the high-quality front contact over the device. The impacts of the nonuniform distribution of R_c on device performance are further investigated using the numerical fitting model presented in Section 3.2.

With the improvement of front contact observed in EL imaging and specific contact resistance measurement, the influence of RTP annealing on the device performance is further characterized by the IV measurement, as shown in **Figure 4**. For the cell before annealing, as shown by the red curve in Figure 4a, the kink shape appears in the IV curve, strongly reducing the FF and hence the efficiency of the cell. This indicates that when concerning the large area device, the nonuniform distribution of contact resistance will seriously lower the overall performance around the maximum power point, therefore, should be carefully treated. The change of characterized parameters after 10, 20, and 30 cycles of RTP annealing are shown in Figure 4b–e. V_{OC} and J_{SC} exhibit no significant change after the RTP treatment. The increasing tendency for efficiency is consistent with FF. With 10 cycles of RTP annealing, the FF increases from 61.32 to 63.53% and after the next 10 cycles of RTP annealing, the FF jumps to 78.50%. This increase brings a significant 5% absolute efficiency improvement which could be attributed to the decreased R_c during the cyclic RTP annealing. Although the CTLM measurement results in Figure 3d based on small localized area show the R_c reduction saturates after 10 cycles of RTP annealing, the further enhancement of FF after 20 cycles of RTP annealing might be due to the

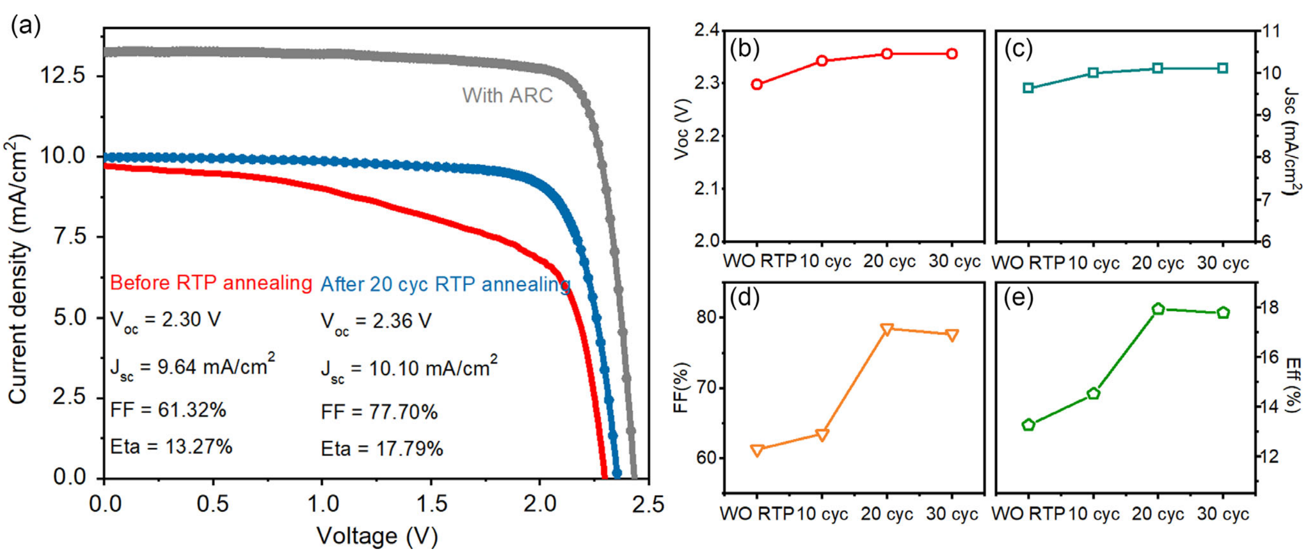

Figure 4. Performance characterizations of the GaInP/GaAs cell before and after cyclic RTP contact annealing a) current–voltage characteristic, b) open-circuit voltage, c) short-circuit current density, d) FF, and e) efficiency.

improvement of low R_c over the whole cell area. After 30 cycles of RTP annealing, a slight drop in FF as well as efficiency is observed for the cell. This drop is likely caused by the damage of the polymer bonding layer after excess cycles of RTP treatment. After 20 cycles of RTP annealing, cell efficiency increases from 13.27 to 17.79%, which is further boosted to 22.30% after ARC deposition, as shown in Figure 4a.

Although RTP annealing can significantly improve cell performance, this process will induce damage to the polymer bonding layer after multiple cycles of treatments due to its limit on heating selectivity. The accumulated heating and cooling during cyclic RTP treatment accelerates the aging of the polymer and therefore restricts the effectiveness of cell performance improvement. To achieve better annealing selectivity on front contact, monochromatic laser annealing is adopted to minimize the heating damage on the polymer bonding layer. A continuous-wave diode laser with a wavelength of 808 nm is used to scan the top surface of the cell for selectively annealing the front side, whose penetration depth is about 1 μm for GaAs.[31] Considering the thicknesses of the GaAs junctions 3 μm and the GaInP junction is about 650 nm, the front metal contact on the GaInP junction could be selectively heated by laser annealing with minimum influence on the polymer bonding layer. In addition, the short exposure time of milliseconds and the scanning feature of the laser offers the advantage of fast heating and cooling which will further reduce the aging effect on the polymer bonding layer.

An optimized laser dose of 12 J cm^{-2} is used to effectively anneal the front contact meanwhile protecting the polymer bonding layer from damage. The improvement of cell performance by laser annealing is characterized by IV measurements. The kink shape in the IV curve is also observed for the device before annealing and is fixed by the laser treatment, as shown in **Figure 5**a. The parameters of the cell before and after laser annealing are shown in Figure 5b–e. The FF rises sharply from 67.15 to 78.80% after twice of laser treatments and further increases gradually to 81.79% after another four cycles. The efficiency rises from 15.89 to 19.73% after six cycles of laser annealing with a similar trend as the FF, whereas V_{OC} and J_{SC} largely remain unimpacted. After the ARC coating, the efficiency of the cell reaches 24.50%. EL images of GaInP junction were also taken after laser annealing to analyze the improvement of front contact. As shown in Figure 5f, six cycles of laser annealing treatment give uniform emission over the whole device area which is much better than the EL result after cyclic RTP shown in Figure 3c. Both IV and EL results show that laser annealing is more effective than the RTP process on front contact annealing and therefore device performance improvement. In addition, the significant increase in device performance after the initial twice laser treatments indicates that laser annealing can effectively heat the metal contact to induce metal diffusion in a very short time without decomposition of the polymer. As the 808 nm laser used in this work can penetrate through the top GaInP junction, the use of a laser with a shorter wavelength within the absorption band of GaInP will lead to a better selectivity for the front side treatment.[32]

3.2. Fitting and Simulation

Simulation is conducted to better understand the mechanism of the device performance improvement resulted from selective contact annealing. A fitting model is established which allows extracting parameters affected by resistance from the measurement results. In the model, the cell performance is simplified as the combined contribution from the area with good contacts $A_{(RC=0)}$ and bad contact A_{RC}, as shown in **Figure 6**a. And an equivalent electrical circuit composed of four subcircuits is applied, as shown in Figure 6b. The bad contact area indicated by the yellow shading area is represented by subcircuits A and B. R_c is the lumped contact resistance at this area. The other part of the cell without the R_c issue is represented by subcircuits C and D. The fraction of the area impacted by the high R_c issue is described by α. The current of the cell is generated by four ideal current sources, and each of them follows the relation of one diode equation

$$J = J_{sc} - J_0 \exp\left(\frac{qV}{kT}\right) \tag{1}$$

where q is the elementary charge, k is the Boltzmann constant, T is the temperature fixed at 300 K, J_{sc} is the photocurrent which

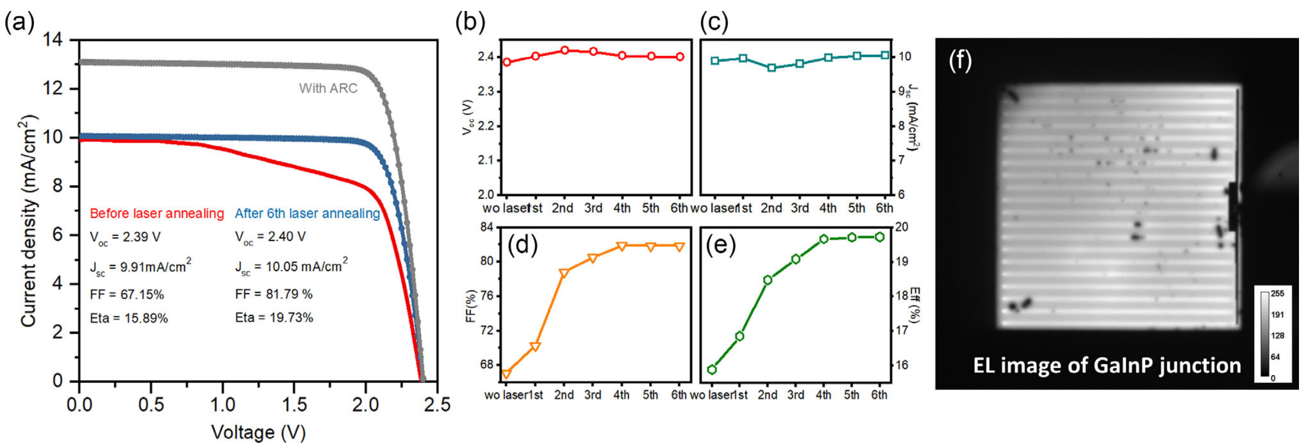

Figure 5. Performance of the GaInP/GaAs cell before and after laser annealing a) current–voltage characteristic, b) open-circuit voltage, c) short-circuit current density, d) FF, e) efficiency, and f) EL image of the GaInP junction after six cycles of laser annealing.

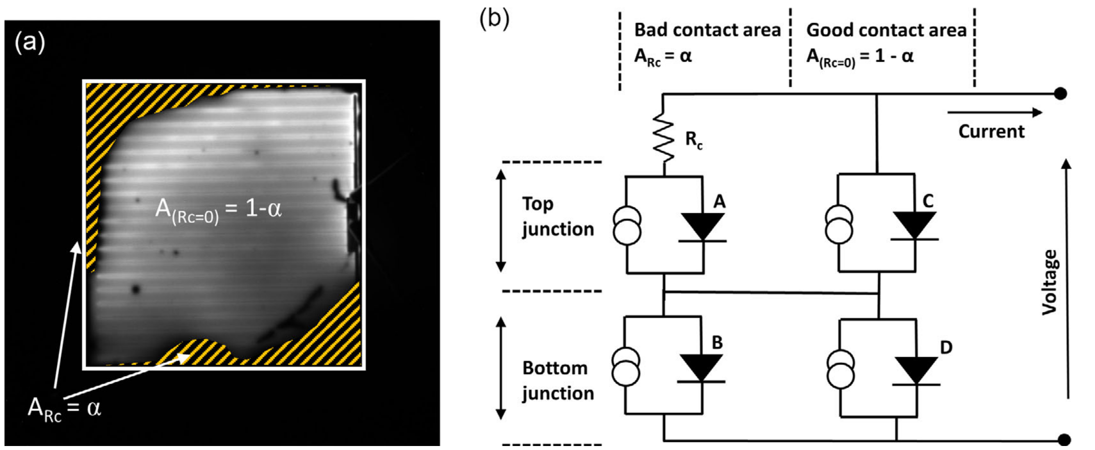

Figure 6. a) Simplified diagram illustrating the device with the nonuniform distribution of contact resistance and b) model of the cell with nonuniform resistance distribution.

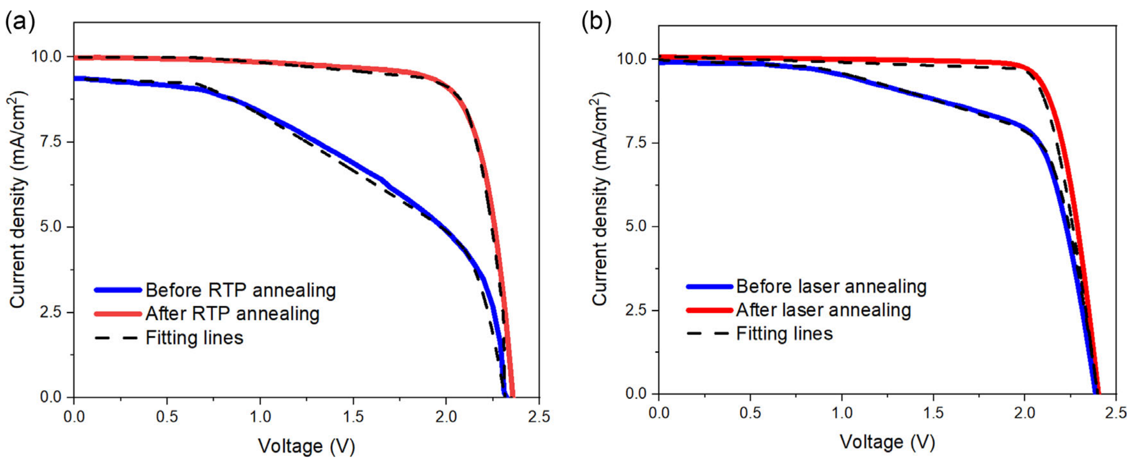

Figure 7. The fitting results with the experimental IV data of a) RTP annealing and b) laser annealing.

is determined by the IV measurement. In the calculation, the recombination current of the top junction $J_{0(A,C)}$ is set as 4.12×10^{-23} mA cm^{-2} and for the bottom junction, $J_{0(B,D)}$ is 2×10^{-16} mA cm^{-2}. Top and bottom junctions are considered as current match, and the shunt resistance is set as an infinite value considering the good crystal quality and low dislocation density of the III–V semiconductor.

The experimental IV curves of the device before and after selective RTP and laser annealing are used here for the fitting. As shown in **Figure** 7a,b, the fitted IV curves agree well with experimental results. For the cell before annealing, the fitting model enables us to analyze the origin of the poor performance by investigating the voltage of each subcircuit. In the voltage range of 0.9–2.0 V, the calculated voltages across subcircuits A (V_A) and C (V_C) of the top junction show a large discrepancy due to the high value of R_c. The specific voltages of subcircuits at the maximum power point of the cell (1.65 V for cell before selective RTP annealing, 2.0 V for cell before selective laser annealing) are shown in **Table 1**, as an example. This nonuniform voltage distribution in the top junction agrees with the

Table 1. Calculated voltages across subcircuits at the maximum power point of cells.

Parameters[a]	Before RTP annealing (V)	Before laser annealing (V)
V_A	1.38	1.39
V_B	0.98	0.99
V_C	0.84	1.22
V_D	0.94	0.93

[a] V_A, V_B, V_C, and V_D refer to the voltage across subcircuit of A, B, C, and D.

Table 2. Calculated parameters of cells before and after cyclic RTP and laser annealing.

Parameters	RTP annealing		Laser annealing	
	Before	After	Before	After
R_c (Ω cm^2)	6.1×10^{-4}	4.8×10^{-4}	5.0×10^{-4}	4.0×10^{-6}
α	0.54	0.08	0.24	0.05

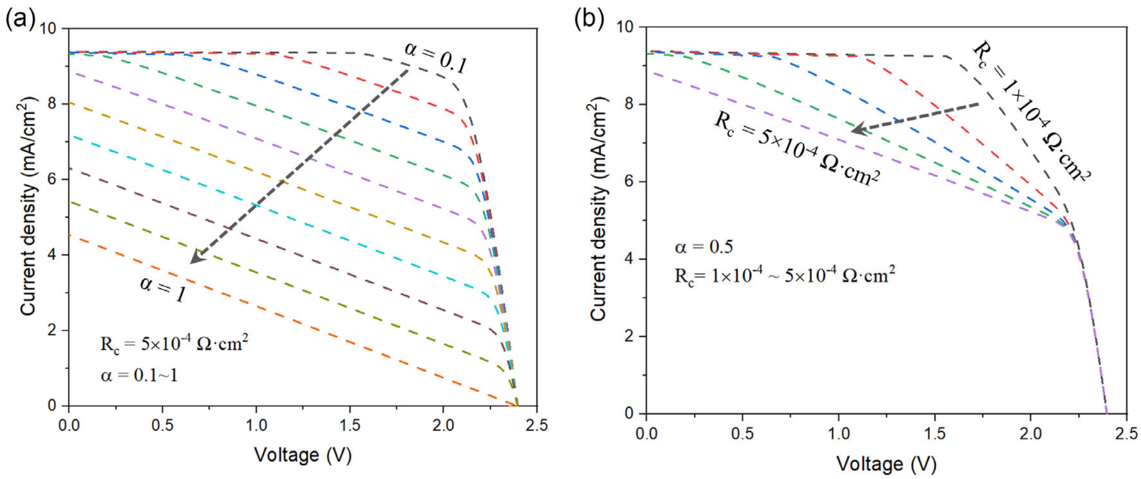

Figure 8. The calculated IV curves with changing a) α and b) R_c.

measured EL image in Figure 2a which exhibits an obvious difference in emission intensity over the cell area. While values of V_B and V_D are more closed with each other which can be attributed to the high doping tunnel junction between the top and bottom junction. Therefore, the EL image of the GaAs junction is less affected by the bad front contact, as shown in Figure 2b.

Furthermore, values of R_c and α of cells before and after RTP and laser annealing are calculated through the IV curves fitting to demonstrate their impacts on device performance. As shown in **Table 2**, after RTP and laser annealing, both R_c and α are decreased which supports the assumption proposed based on EL and IV measurement results. Furthermore, the laser annealing demonstrates more effectiveness according to the calculation. After the laser annealing, the bad contact area is reduced to only 0.05 of the overall device area and the R_c at this area is as low as $4.0 \times 10^{-6}\ \Omega\, cm^2$ which is low enough for the high-performance solar cells.

In addition to fitting the experimental data, the built model enables us to quantitatively investigate the impact of the R_c and α on the device performance. As shown in **Figure 8**a, with $R_c = 5.0 \times 10^{-4}\ \Omega\, cm^2$ and increasing α from 0.1 to 1, the IV curves move parallelly toward the zero point. And the FF drops from 77.70 to 12.21% linearly. Although with $\alpha = 0.5$ and increasing the R_c from 1.0×10^{-4} to $5.0 \times 10^{-4}\ \Omega\, cm^2$, the slope of the kink shape on the IV curves is changed, as shown in Figure 8b. The result indicates that for the device with nonuniform contact resistance, both values of R_c and α will significantly impact the IV performance of the device in different ways and result in the kink shape. Furthermore, when R_c is equal to $5.0 \times 10^{-4}\ \Omega\, cm^2$ and α is equal to 0.5, the IV curve is similar to the cell with low shunt resistance.

Using the fitting model, the impact of selective annealing on device performance improvement through reducing R_c and α is revealed. Moreover, the fitting parameters confirm that laser annealing with better selectivity is more effective to form the high-quality front contact compared with RTP annealing. In addition, the built model enables the analysis of the impact from R_c and α and implies that the R_c changes the FF linearly and α changes the slope of the kink shape.

4. Conclusion

This study demonstrates the developed selective contact annealing can effectively improve the performance of bifacial-grid III–V thin-film cells bonded on glass through the reduction of contact resistance (R_c) and the bad contact fraction (α). Before annealing treatment, low-quality front contact is revealed using the combination of PL and EL imaging methods. Selective contact annealing processes utilizing RTP or laser to reduce the contact resistance at the metal/semiconductor interface are used, leading to a remarkable improvement of the device performance. We found the laser method is more effective than RTP in terms of front contact treatment due to its better selectivity. A fitting model of the cell with nonuniformly distributed resistance is built to investigate the mechanism of selective contact annealing which verifies that the enhanced device performance is attributed to the suppression of R_c and α. This work demonstrates an effective annealing approach to fabricate high-quality metal–semiconductor contacts for the device with poor thermal resistivity, which can be used in Si-based tandem solar cells bonded by polymer and other flexible optoelectronic semiconductor devices on polymer substrates.

Supporting Information

Supporting Information is available from the Wiley Online Library or from the author.

Acknowledgements

C.L. and H.W. contributed equally to this work. The authors acknowledge Yihao Wang and Heng Sun for their assistance in EL image measurements and acknowledge Mingxv Jiang and Arman Mahboubi Soufiani for helpful discussion.

Conflict of Interest

The authors declare no conflict of interest.

Data Availability Statement

Research data are not shared.

Keywords

bifacial-grid III–V solar cells, laser annealing, metallization, tandem solar cells

Received: June 23, 2021
Revised: August 16, 2021
Published online:

[1] T. J. Grassman, D. J. Chmielewski, S. D. Carnevale, J. A. Carlin, S. A. Ringel, *IEEE J. Photovoltaics* **2016**, *6*, 326.
[2] M. Feifel, D. Lackner, J. Ohlmann, J. Benick, M. Hermle, F. Dimroth, *Sol. RRL* **2019**, *3*, 1900313.
[3] M. Feifel, D. Lackner, J. Ohlmann, K. Volz, T. Hannappel, J. Benick, M. Hermle, F. Dimroth, *Conf. Rec. IEEE Photovoltaic Specialists Conf.*, IEEE, Piscataway, NJ **2020**, p. 0194.
[4] R. Cariou, J. Benick, F. Feldmann, O. Höhn, H. Hauser, P. Beutel, N. Razek, M. Wimplinger, B. Bläsi, D. Lackner, M. Hermle, G. Siefer, S. W. Glunz, A. W. Bett, F. Dimroth, *Nat. Energy* **2018**, *3*, 326.
[5] D. Lackner, O. Höhn, R. Müller, P. Beutel, P. Schygulla, H. Hauser, F. Predan, G. Siefer, M. Schachtner, J. Schön, J. Benick, M. Hermle, F. Dimroth, *Sol. RRL* **2020**, *4*, 2000210.
[6] S. Essig, M. A. Steiner, C. Allebé, J. F. Geisz, B. Paviet-Salomon, S. Ward, A. Descoeudres, V. LaSalvia, L. Barraud, N. Badel, A. Faes, J. Levrat, M. Despeisse, C. Ballif, P. Stradins, D. L. Young, *IEEE J. Photovoltaics* **2016**, *6*, 1012.
[7] S. Essig, C. Allebé, T. Remo, J. F. Geisz, M. A. Steiner, K. Horowitz, L. Barraud, J. S. Ward, M. Schnabel, A. Descoeudres, D. L. Young, M. Woodhouse, M. Despeisse, C. Ballif, A. Tamboli, *Nat. Energy* **2017**, *2*, 17144.
[8] L. Wen, F. Gao, S. Zhang, G. Li, *Small* **2016**, *12*, 4277.
[9] F. Gao, G. Li, *Appl. Phys. Lett.* **2014**, *104*, 042104.
[10] L. Wen, F. Gao, Y. Yu, Z. Xu, Z. Liu, P. Gao, S. Zhang, G. Li, *J. Mater. Chem. A* **2018**, *6*, 17361.
[11] M. A. Green, E. D. Dunlop, J. Hohl-Ebinger, M. Yoshita, N. Kopidakis, X. Hao, *Prog. Photovoltaics Res. Appl.* **2020**, *28*, 629.
[12] M. M. R. Howlader, P. R. Selvaganapathy, M. J. Deen, T. Suga, *IEEE J. Sel. Top. Quantum Electron.* **2011**, *17*, 689.
[13] P. H. Hao, L. C. Wang, F. Deng, S. S. Lau, J. Y. Cheng, *J. Appl. Phys.* **1996**, *79*, 4211.
[14] T. Potthoff, K. Bothe, U. Eitner, D. Hinken, M. Königes, *Prog. Photovoltaics Res. Appl.* **2010**, *18*, 100.
[15] H. Cotal, C. Fetzer, J. Boisvert, G. Kinsey, R. King, P. Hebert, H. Yoon, N. Karam, *Energy Environ. Sci.* **2009**, *2*, 174.
[16] M. Kato, Y. Okinaka, *Gold Bull.* **2004**, *37*, 37.
[17] A. U. Rehman, S. H. Lee, *Solar Cells-New Approaches and Reviews*, IntechOpen, London **2015**.
[18] A. Rohatgi, Z. Chen, P. Doshi, T. Pham, D. Ruby, *Appl. Phys. Lett.* **1994**, *65*, 2087.
[19] G. D. Mooney, A. M. Hermann, J. R. Tuttle, D. S. Albin, R. Noufi, *Appl. Phys. Lett.* **1991**, *58*, 2678.
[20] B. Rau, T. Weber, B. Gorka, P. Dogan, F. Fenske, K. Y. Lee, S. Gall, B. Rech, *Mater. Sci. Eng. B* **2009**, *159–160*, 329.
[21] J. Dore, S. Varlamov, R. Evans, B. Eggleston, D. Ong, O. Kunz, J. Huang, U. Schubert, K. H. Kim, R. Egan, M. Green, *EPJ Photovoltaics* **2013**, *4*, 40301.
[22] A. Queraltó, A. Pérez Del Pino, M. De La Mata, M. Tristany, X. Obradors, T. Puig, S. Trolier-McKinstry, *Ceram. Int.* **2016**, *42*, 4039.
[23] Z. Liu, X. Hao, J. Huang, W. Li, A. Ho-Baillie, M. A. Green, *Thin Solid Films* **2016**, *609*, 49.
[24] H. Kwon, W. Choi, D. Lee, Y. Lee, J. Kwon, B. Yoo, C. P. Grigoropoulos, S. Kim, *Nano Res.* **2014**, *7*, 1137.
[25] J. J. Schemer, P. Mulder, G. J. Bauhuis, P. K. Larsen, G. Oomen, E. Bongers, *Prog. Photovoltaics Res. Appl.* **2005**, *13*, 587.
[26] J. Rechid, K. Heime, *Solid State Electron.* **2000**, *44*, 451.
[27] I. Lombardero, C. Algora, *Sol. Energy Mater. Sol. Cells.* **2020**, *204*, 110236.
[28] S. Bowden, A. Rohatgi, *17th European Photovoltaic Solar Energy Conf.*, Georgia Tech Library, Munich, Germany **2001**, *91*, p. 1698.
[29] R. Williams, *Modern GaAs Processing Methods*, Artech House Microwave Library, suburban Boston **1990**.
[30] G. J. Bauhuis, P. Mulder, E. J. Haverkamp, J. C. C. M. Huijben, J. J. Schermer, *Sol. Energy Mater. Sol. Cells.* **2009**, *93*, 1488.
[31] G. E. Jellison Jr, *Opt. Mater.* **1992**, *1*, 151.
[32] H. J. Kwon, S. Kim, J. Jang, C. P. Grigoropoulos, *Appl. Phys. Lett.* **2015**, *106*, 113111.

